Wang, J., Pozegic, T., Xu, Z., Nigmatullin, R., Harniman, R., & Eichhorn, S. J. (2019). Cellulose nanocrystal-polyetherimide hybrid nanofibrous interleaves for enhanced interlaminar fracture toughness of carbon fibre/epoxy composites. *Composites Science and Technology*, *182*, [107744]. https://doi.org/10.1016/j.compscitech.2019.107744

Cellulose nanocrystal-polyetherimide hybrid nanofibrous interleaves for enhanced interlaminar fracture toughness of carbon fibre/epoxy composites

Jing Wang[a], Thomas R. Pozegic[a], Zhen Xu[b], Rinat Nigmatullin[a], Robert L. Harniman[c], Stephen J. Eichhorn [a]*

[a] *Bristol Composites Institute (ACCIS), School of Civil, Aerospace and Mechanical Engineering, University of Bristol, University Walk, Bristol BS8 1TR, UK.*

[b] *Department of Chemical Engineering, Imperial College London, South Kensington Campus, London SW7 2AZ, UK.*

[c] *School of Chemistry, University of Bristol, Cantock's Close, Bristol BS8 1TS, UK.*

Abstract

The effect of electrospun cellulose nanocrystals (CNCs)-polyetherimide (PEI) hybrid nanofibrous mats on Mode I and Mode II interlaminar fracture toughness of unidirectional carbon/epoxy composite laminates is demonstrated. It is shown that the CNCs reinforced PEI nanofibrillar interleaves result in a ~28% increase in Mode I initial fracture toughness values compared to neat PEI nanofibrous interleaves. Specifically, the interrelated micro- and nano-scale toughening mechanisms including carbon fibre bridging, fibre necking, fibre rupture with CNCs aggregates, and nanofibre rupture contributed to the fracture toughness improvements under Mode-I loading. Nano-scale mechanisms of shear hackles, and crack pinning by CNCs aggregates increased the Mode II fracture toughness up to ~3 kJ/m^2 as a result of a 6 wt.% CNCs reinforced PEI nanofibrillar mat interleaves. Interleaving laminated composites with electrospun CNCs-PEI hybrid nanofibrillar mats has been demonstrated as a novel and prospective strategy to strengthen and toughen interlaminar zones of carbon/epoxy composite laminates.

Keywords: Delamination; Fracture toughness; Electrospinning; Cellulose nanocrystals

*Corresponding Author: Email: s.j.eichhorn@bristol.ac.uk; Tel: +44(0)11733156050.

1. Introduction

Currently, interlaminar delamination [1] is the most prevalent failure modes limiting the wider applications of carbon fibre reinforced polymers (CFRPs) in a variety of fields [2]. The critical strain energy release rate (G_C) and interlaminar fracture toughness are fundamental parameters characterising the resistance of composites to delamination growth and to evaluate interlaminar fracture performance [3]. One of the most effective techniques for enhancing resistance to interlaminar delamination and fracture toughness is interleaving. This typically consists of inserting a tough thermoplastic layer between the plies, without adding additional composite thickness; it can be described as a discrete secondary matrix layer in the form of particles, films or fibres [4]. Nanofibrous interleaves avoid problems such as processing high viscosity polymers [5], increasing the laminate thickness, loss of in-plane performances [6], poor resin flow and adhesion to the epoxy resin relative to the particulate or film-based interleaf [7].

Electrospinning (ES) is an efficient and simple technique for producing nanofibrous polymer mats or nanofibril mats, with large specific surface area, high porosity (>80%), and good continuity [8]. Most importantly, ES can assist with the integration of nanomaterials to fabricate nanocomposites in a one-step and controllable process. Dzenis [9] proposed a toughening mechanism of entangled electrospun nanofibres as a secondary nano-reinforcement to improve interlaminar fracture toughness, whereby nanofibres bridge the crack, much like the loops and hooks found in Velcro. It was found that the nanocomposites absorbed additional energy *via* nanoscale and microscale toughening mechanisms once the surrounding epoxy resin fractures. Hamer *et al*. [10] reported the effect of multi-wall carbon nanotubes (MWCNTs) as nano-reinforcements for improving the G_{IC} of nylon 6,6 nanofibrous mats interleaved in plain woven composite laminates.

They reported that Mode I and II critical strain energy release rates (G_{IC} and G_{IIC})-fracture energy were enhanced by 25% and 20%, respectively, compared with neat nylon 6,6 interleaved laminated composites. The addition of MWCNTs promoted the formation of a plastic zone near the crack tip. Eskizeybek *et al.* [11] studied CNTs-polyacrylonitrile (PAN) electrospun nanofibres interleaves in carbon/epoxy laminated composites under Mode I loading. They reported that the G_C at a stable crack propagation- $G_{IC,propagation}$ ($G_{IC,prop}$) of PAN-3wt.% CNT samples demonstrated a 45% increase with respect to that of neat PAN, but concluded that PAN-5wt.% CNT had a lower performance on G_{IC} due to the agglomeration of CNTs [12]. Cellulose is the most abundant renewable organic resource on the planet. Over the past few decades, CNCs have attracted extensive attention as a reinforcement phase in polymer nanocomposites on account of their high aspect ratio of 5-30 (typically 50-350 nm in length, 5-20 nm in width) [13], high crystallinity (54-88%), tensile strengths ranging from 7.5 - 7.7 GPa and Young's modulus in axial direction ranging from 110 to 220 GPa [14]. As an alternative to non-biodegradable CNTs, CNCs possess additional advantages of potential biodegradability, sustainability and large-scale availability at relatively low cost [15]. Gong et al. [16] have reported that an addition of 2 wt.% CNC into polyvinyl acetate (PVA) matrix could result in a 200% increase in the fracture toughness compared with that of neat PVA.

In this work, polyetherimide (PEI) was combined with CNCs. PEI was chosen for its relatively high Young's modulus of ~3 GPa and a relatively high T_g of 217 ℃ [17], with the ether linkage enhancing the processing ability, and the imide ring offering good mechanical properties and thermal stability [18]. Electrospun CNCs/PEI nanofibrous interleaves are easy to process resulting in a three-dimensional nano-scale high porosity network. Furthermore, they contain CNCs with unique properties such as a high aspect

ratio, large interfacial area, which translate into reinforced epoxy composites with significant energy absorption potential, thus enhancing the interlaminar fracture energy of composite laminates. To the best of our knowledge, it is the very first report on CNCs reinforced polymer as hybrid nanofibrous interleaves for carbon fibre/epoxy composites with enhanced interlaminar fracture toughness.

2. Experimental

2.1. Materials

Unidirectional (UD) carbon fibre/epoxy prepregs composed of HexTow IM7 carbon fibre of weight/length of 0.446 g/m and HexPly 8552 (high performance tough epoxy matrix), were both obtained from Hexcel. PEI (ULTEM® 1000) and 1-methyl-2-pyrrolidone (NMP) were purchased from Sigma-Aldrich and used as received. Whatman no.1 filter paper was used to produce CNCs, and sulfuric acid (95 wt.%) was obtained from Fisher Chemicals (UK). Hydrochloric acid (37 wt.%), and sodium hydroxide pellets (laboratory reagent grade) were both purchased from Fisher Chemicals (UK).

2.2. Preparation of cellulose nanocrystals

Shredded No 1 filter paper (5.2 g) from Whatman was placed in a 500 mL beaker kept in an ice bath, then 104 mL of 60 wt.% sulfuric acid aqueous solution was added dropwise to the cellulose resulting in acidic phase/pulp ratio of 20 ml/g. After the required amount of sulphuric acid was added, the reaction mixture was kept at 45 °C for 1 h under stirring. After hydrolysis, the reaction product was isolated using centrifugation at 10,000 rpm for 6 min (Heraeus Multifuge Xl, Thermo Fisher®). The suspension was transferred into dialysis tubing and dialysed against DI water for 3-5 days with a daily exchange of water until the pH value was around 6.4. The final suspension was subsequently tip sonicated for 15 min at an amplitude of 15% using an ultrasonicator (Branson Digital Sonifier®)

with the sample cooled in an ice bath. Dried CNCs were obtained *via* a freeze dryer (Freezone 2.5, LABCONCO®); the yield of CNCs was found to be ~50%. The preparation of CNCs from filter paper is schematically presented in Supplementary Information (SI) (Fig. S1and S2).

2.3. Electrospinning of nanofibrous interleaves

2 g of PEI were initially dissolved in 20 mL of NMP under stirring for 12 h. CNCs at concentrations of 3 and 6 wt.% with respect to PEI, were added to this primary PEI solution (ca 1 wt.%) and dispersed under tip sonication at 15% power. After sonication, an additional 3.14 g of PEI were added into the primary PEI solution with dispersed CNCs and allowed to dissolve for 12 h under stirring to obtain a PEI solution of a final concentration of 20 wt.% containing dispersed CNCs. Consequently, three types of spinning solution were prepared: neat PEI, 3 wt.% CNC-PEI, and 6 wt.% CNC-PEI. Spinning solutions were loaded into a 10 mL glass syringe with a luer lock metal nozzle and a 21-gauge stainless steel needle (inner diameter 0.8 mm, Socorex). The injection needle was connected to a high-voltage power supply (Linari Engineering) that providing a DC voltage of 17.0 kV. A flow rate or injection speed of 0.625 mL h^{-1} was used to deliver the solution by a syringe pump to the needle tip. The distance between the needle tip and collector was set to 20 cm. Three types of nanofibrous mats were produced at the areal weights of 4.70 ± 1.50 g m^{-2}, all collected on the aluminium foils.

2.4. Composite laminates production

Neat PEI, 3 wt.% CNC-PEI and 6 wt.% CNC-PEI nanofibres interleaved in the mid-plane within a UD $[0]_{24}$ composite laminate was produced with IM7/8552 carbon fibre/epoxy prepregs (300 × 300 mm) (SI, Fig. S3). The thin polyimide (PI) film with a thickness of 20 μm and length of 50 mm was inserted at the mid-plane of the laminates

to form an initial site for delamination. Neat PEI, 3 wt.% CNC-PEI and 6 wt.% CNC-PEI nanofibrous mats of the desired dimensions were removed from the aluminium foil substrate using the 'sticky' prepreg. The laminates were then placed into an autoclave (Leeds and Bradford Boiler Company Limited), applying a vacuum at 1 bar and then 7 bar gauge, finally reducing to 0.2 bar. The curing cycle was continued at a heating rate of 3 °C min^{-1} from room temperature to 110 °C and was held at this value for 1 h, followed by a post curing process at 180 °C for another 2 h. Unidirectional carbon fibre/epoxy laminates with neat PEI, 3 wt.% CNC-PEI and 6 wt.% CNC-PEI nanofibrous interleaves in the mid-plane, were denoted as PEI, PEI3, PEI6 specimens, respectively.

2.5. Interlaminar fracture mechanics tests

2.5.1. Mode I test

DCB specimens were produced with the following dimensions: 140 mm long, 20 mm wide, 3.2 mm thick. Piano hinges of width of 20 mm and a front length of 25 mm were attached to the specimens, and testing was carried out in accordance to ASTM D5528. DCB tests were performed using a Shimadzu AGS-X tensile tester fitted with 10 kN load cell. Tests were conducted at a constant crosshead speed of 1 mm min^{-1} and a load data rate of 10 Hz. A pre-crack of length 5 mm was formed after the PI film tip while the specimen was unloaded. The process of crack propagation and the load and displacement was monitored *via* a high-resolution DSLR camera in video mode at increments of every 1 mm for the first 5 mm and every 5 mm subsequently (SI, Fig. S4a). At least three specimens were tested for each type of nanofibrous mat interleaved composites. Modified beam theory (MBT), as stated in the ASTM D5528 standard, was used to calculate $G_{IC,ini}$ and $G_{IC,prop}$ using the equation:

$$G_I = \frac{3P\delta}{2b(a+|\Delta|)} \quad (1)$$

where G_I is the Mode I strain energy release rate, P is the applied load, δ is the load point displacement, b is the specimen width, a is the delamination length (distance from the applied point to the crack tip) and Δ is the *x*-intercept in the plot of the cube root of the compliance ($C = \delta/P$), $C^{1/3}$, as a function of a.

2.5.2. Mode II test

ENF specimens with dimensions of 160 × 20 × 3.2 mm, a span length (*2L)* of 100 mm, one loading roller and two support rollers with the radius of 5 mm were prepared as the ASTM D7905 standard test method [19]. ENF tests were performed using a Shimadzu AGS-X testing machine fitted with a 10 kN load cell. Testing was conducted at a constant crosshead rate of 1 mm min^{-1} and load and displacement data were recorded at rate of 100 Hz. The specimens were positioned at a constant distance of 30 mm between the centre of the support roller and the PI film tip so the ratio of the crack length to half span (*a/L*) was 0.6. The load-displacement values were recorded during each test, and the crack tip was observed *via* a video gauge (SI, Fig. S4b). Three specimens at least were tested for each type of nanofibrous mats interleaved composites. Euler Bernoulli beam theory was adopted in this work, which has been applied in the ENF fracture toughness by several researchers [2, 11, 20, 21]:

$$G_{IIC} = \frac{9a^2 P_C \delta}{2B(2L^3+3a^3)} \quad (2)$$

where P_C is the maximum load during the test, *B* is the specimen width and *L* is the half span-length.

2.6. Characterisation methods

The morphology of the prepared CNCs was observed using a transmission electron microscope (TEM, JEOL 1400). The sample was prepared by depositing a CNC aqueous suspension with a concentration of 0.015 wt. % on carbon-coated TEM grid. Fourier-

transform infrared (FTIR) spectra of PEI, CNCs, 3 wt.% CNC-PEI and 6 wt.% CNC-PEI were acquired using FT-IR spectrometer (Spectrum Two, PerkinElmer®) fitted with a universal ATR accessory. The thermal stability of the CNC particles and the mats of PEI, 3 wt.% CNC-PEI and 6 wt.% CNC-PEI (5-10 mg) was studied by thermogravimetric analysis (TGA) / differential scanning calorimetry (DSC) STA (449 F3, Jupiter®) at a 10 K min^{-1} heating rate from 25 to 625 °C under a nitrogen environment (50 ml min^{-1}). AFM imaging was conducted using a Multi-Mode VIII microscope with Nanoscope V controller operating under non-resonant PeakForce feedback control (Bruker, CA, USA). Tensile tests were carried out using a tensile stage controller (DEBEN®) with a 5 N load cell at a crosshead speed of 0.5 mm/min. Optical microscopy (Imager M2, ZEISS®) was used to determine the crack path on a polished cross-section of the post-tested PEI, PEI3 and PEI6 specimens. A scanning electron microscope (SEM, JEOL IT300) at 15.0 kV was used to investigate the surface morphologies of neat PEI, 3 wt.% CNC-PEI and 6 wt.% CNC-PEI nanofibrous mats and fracture surfaces of tested specimens.

3. Results and discussion

3.1. Morphology of nanofibrous mats

Fig. 1(a-b) show typical TEM images of prepared CNCs. They are rod-shaped, with diameters in the range of 7 to 12 nm and lengths between 170 nm and 220 nm. The hydrolysis process generates sulphate half-ester groups on the CNCs surface, which have a negative charge. These groups facilitate a stable dispersion of the CNCs in an aqueous solution. The surface charge density of CNCs produced was found to be 82.3 ± 0.7 mmol kg^{-1} *via* a conductometric titration. Typical SEM images of the as-spun neat PEI, 3 wt.% CNC-PEI and 6 wt.% CNC-PEI nanofibrous mats are presented in Fig. 1(c-h). It is observed that all fabricated nanofibres are randomly oriented with a homogenous and

entangled three-dimensional network structure. The addition of the 3 wt.% CNCs leads to the average fibre diameter decreasing to ~800 nm from ~1.3 μm of the electrospun neat PEI average nanofibres diameter. At 6 wt.% CNCs, the nanofibres diameter significantly decreases to ~400 nm. This is attributed to the enhanced charge density or electrostatic force with increased CNCs content, causing the fibres to be stretched to a greater degree when the nanofibres jets are ejected away from the needle [22]. In addition, a small number of beads are observed in hybrid nanofibres, which could be prevented with increasing charge density (Fig. 1g).

3.2. Characteristics of nanofibrous mats

FTIR spectra of the electrospun nanofibrous mats and prepared CNCs particles were obtained (see SI, Fig. S5a). CNC characteristic band at ~2900 cm^{-1}, attributed to C–H bonds stretching [22], was broadened with an increasing addition of CNCs in hybrid nanofibres, though it overlaps with an absorbance peak from the PEI. A typical absorption band of pure PEI nanofibers at ~1720 cm^{-1} due to symmetric stretching vibrations of the imide carbonyl group, decreased in intensity with an increase of CNCs content in hybrid nanofibres. Therefore, hybrid electrospun nanofibres are a physical mixture and no chemical reactions are expected between PEI and CNCs. The presence of CNCs in composites was also revealed by thermal response in TGA experiments (see SI, Fig. S5b). Neat PEI nanofibers and CNCs exhibited a single-step weight loss with T_{onset} at 510 °C [23] and at 278 °C, respectively. However, CNCs/PEI nanofibrous mats have a two-step thermal decomposition which became more obvious with an increase in the CNC content. Interestingly, the decomposition temperature of PEI matrix for 3 wt.% and 6 wt.% CNC-PEI nanofibres were elevated to 515 and 512 °C, respectively, indicating a slight enhancement of thermal stability with the addition of CNCs. To visualise the distribution

of CNCs in the PEI matrix, high resolution AFM images were obtained for longitudinal and transverse sections of electrospun composite fibres prepared by microtome sectioning of nanofibrous mat embedded into a resin (Fig. 2) Distinguishing of two composite entities was possible using "error signal" imaging, which emphasises the interfaces, and phase imaging, which probes materials stiffness. The modulus of PEI ranges from 3.20 to 3.45 GPa while values for CNCs range from 110 to 220 GPa; therefore the dark blue area indicates the presence of CNCs on this basis (see Fig. 2b,d). Both types of imaging indicate a uniform distribution of CNCs in the PEI nanofibre with only a small fraction of aggregates. It appears that CNCs are randomly oriented in the polymer matrix. A smaller number of elongated nanoparticles were observed in the transverse section reflecting a low probability of the orientation of CNCs perpendicular to the nanofiber length. Consequently, the rod-shaped CNCs were uniformly distributed within the PEI nanofibres which is believed to realize the bridging of cracks v*ia* a structured network.

3.3. Tensile properties of the nanofibrous mats

Fig. 3a shows three typical stress-strain curves for PEI-based nanofibrous mats. The tensile strength and modulus of the PEI-based nanofibrous mats are calculated as presented in Fig. 3b and SI, Table S1. The neat PEI nanofibrillar mat has a tensile strength of 0.56 ± 0.09 MPa, and the value is increased by 20% to 0.67 ± 0.13 MPa with the addition of 3 wt.% CNCs. Increasing the CNCs loading to 6 wt.% enhances the tensile strength to 0.63 ± 0.07 MPa, yielding 13% improvement compared to that of neat PEI. Simultaneously, the tensile modulus of neat PEI nanofibres is calculated as 17.55 ± 3.75 MPa. The tensile modulus of 3 wt.% CNC-PEI nanofibres demonstrates a significant enhancement of the stiffness, up to 25.65 ± 4.25 MPa which is attributed to CNCs reinforcement. The tensile modulus of 6 wt.% CNC-PEI hybrid nanofibres only increases

to 20.48 ± 3.12 MPa due to the aggregations of CNCs in PEI at a higher loading of CNCs. Therefore, CNCs that are strong and stiff natural biopolymers would strengthen and toughen the neat PEI nanofibres as effective reinforcing nano-fillers for interleaved composites laminates.

3.4. Evaluation of the fracture toughness

3.4.1. Mode I fracture toughness

Fig. 4a shows a typical load-displacement curves for interleaved DCB specimens during the pre-crack testing and test loading. For the pre-crack loading, its function is to make the pre-crack sharp to simulate crack development accurately. Typical load-displacement curves for PEI, PEI3, PEI6 specimens under the test loading are shown in Fig. 4b. DCB resistance curves (R-curves) are presented in Fig. 4c, after calculating the G_I data from the corresponding load and displacement and $|\Delta|$ from the intercept using the MBT method (SI, Fig. S6) and Eq. (1). The Mode I fracture energy at the crack initiation ($G_{IC,ini}$) for each type of specimens is defined at the first 1 mm point after the pre-crack (31 mm) is created, and the value at a stable crack propagation ($G_{IC,prop}$) is identified as the average of points beyond the crack length associated with $G_{IC,ini}$ (32-80 mm). The configuration for the Mode I test is displayed in Fig. 5a. The mean and standard deviation (error bars) for F_{max}, $G_{IC,ini}$ and $G_{IC,prop}$ are calculated and presented in Fig. 5b and SI, Table S2. Electrospun 3 wt.% CNC-PEI nanofibres interleaved specimens showed the highest maximum force and $G_{IC,prop}$ among the three types of nanofibrous mats, resulting in a 20% increase and 3% increment in $G_{IC,ini}$, and $G_{IC,prop}$ respectively compared with neat PEI specimens. PEI6 specimens show a 28% increase of $G_{IC,ini}$ due to the nano-reinforcement of CNCs while a 1% decrease occurs for $G_{IC,prop}$ compared to

neat PEI specimens. This decrease is attributed principally to the CNCs' aggregation in PEI nanofibres at a higher loading of CNCs.

With respect to published work, Beckermann *et al.* [4] used electrospun polyamide (PA) 6,6 nanofibres mat distributed with nano-scale $AgNO_3$ precipitates as interleaves for carbon/epoxy composite laminates. They reported that $G_{IC,ini}$ improved by 17% while $G_{IC,prop}$ decreased by 8% compared to non-interleaved specimens under Mode I loading. This trend was similarly observed in this work, with the enhancement in $G_{IC,ini}$ and a small decrease in $G_{IC,prop}$ for Mode I fracture toughness. Furthermore, Brugo and Palazzetti [24] reported fracture toughness enhancement for UD laminates at initiation, with negligible improvement at a propagation stage. This was attributed to the transition of the crack path from the toughened interlayer to the non-toughened interlayer/base lamina interface after crack growth has been initiated. Hence, as stated by Beckermann *et al.* [4], the value for $G_{IC,prop}$ is not a key parameter for evaluating Mode I fracture toughness while the values for $G_{IC,ini}$ have been used to evaluate and compare the interlaminar fracture performance of composite laminates.

3.4.2. Mode II fracture toughness

Fig. 4d shows a typical load vs. displacement curve for electrospun PEI, 3 wt.% CNC-PEI and 6 wt.% CNC-PEI nanofibres interleaved ENF specimens. $G_{IIC,ini}$ for three types of specimens are calculated using Eq. (2); the data were taken from the load - displacement curve and the new delamination lengths. The configuration for Mode II test is displayed in Fig. 5c. The average value and standard deviation (error bars) for F_{max}, $G_{IIC,ini}$ are shown in Fig. 5d and SI, Table S3. The average $G_{IIC,ini}$ values for PEI3 and PEI6 specimens reach 2.678 ± 0.142 and 2.843 ± 0.111 kJ/m^2 respectively, with presenting the highest maximum force for PEI6 specimens. The introduction of 3 wt.%

and 6 wt.% CNCs within PEI nanofibrous interleaves result in 13% and 20% increases in $G_{IIC,ini}$ values with respect to neat PEI specimens, respectively. With regards to the results of Mode I $G_{IC,ini}$, $G_{IIC,ini}$ also had a positive correlation with the increasing content of CNCs. Kostopoulos *et al.* [25] reported that carbon nanofibres and zieconate titanate piezo-electric particles increased the value of G_{IIC} to 2.181 ± 0.100 kJ m^{-2} for composite laminates because of different toughening and energy absorption mechanisms in the distinct phases. Daelemans *et al.* [26] reported the effect of areal weight on enhancing G_{IIC} for composite laminates, and nanofibrous mats composed of PA 6,9 at an areal weight of 18.0 g m^{-2} and obtained a 71% increase in $G_{IIC,ini}$ compared to nanofibrous mats with an areal weight of 3.0 g m^{-2}.

3.5. Toughening mechanisms

3.5.1. Mode I mechanisms

In order to expound the crack path behaviour during Mode I loading, cross-sectional analysis was conducted on the PEI, PEI3 and PEI6 specimens after testing and typical images are displayed in Fig. 6. It is apparent from Fig. 6a that a tortuous delamination path with continual deflections are observed in the PEI sample, signifying potential fracture absorption during carbon fibre/epoxy debonding. The crack crosses from a toughened interlayer and then propagates along the intralaminar region of PEI3 specimens (Fig. 6b). This also suggests a larger deflection and the twisting of the crack path, resulting in increased fracture energy absorption. Similarly, carbon fibre/matrix debonding is observed for PEI6 samples (Fig. 6c) with a similar crack path into the intralaminar area as for PEI3 specimens. Particularly, intra-ply failure is identified as the formation of islands in Fig. 6b-c; thus the intra-ply region has less resistance to crack

growth than through the tougher nanofibrous mats. Typical islands are only seen for PEI3 and PEI6, leading to an increased $G_{IC,prop}$ for PEI3 as a result of its larger island than for PEI6.

The fracture surfaces of tested specimens were investigated *via* SEM images, as shown in Fig. 7. A potential explanation for the relatively large growth of $G_{IC,0}$ (the non-linear point during the first loading – see Fig. 4a) and $G_{IC,prop}$ (Fig. 4c), could be a result of carbon fibres bridging (Fig. 7a) between two 0^o unidirectional plies from the halves of PEI samples [27]. Micro-scale toughening mechanisms such as carbon fibre/matrix debonding and fibre bridging are thought to contribute to the increase in fracture energy. It is observed in PEI specimens (Fig. 7d) that partial nanofibres have been pulled out from the epoxy resin and ruptured without deformation. However, the fracture surfaces of the PEI3 and PEI6 specimens are rougher than that of PEI specimens, which implies the larger effective surface area due to the presence of CNCs nano-reinforcements or aggregates (Fig. 7e,f). This may result in the formation of percolated networks by the aggregation of CNCs, increasing the strength and stiffness of CNCs/PEI nanocomposites [28]. Therefore, tougher CNCs/PEI specimens would require additional plastic deformation (strain) prior to crack initiation compared to PEI neat specimens [29], providing the higher $G_{IC,ini}$ values for the PEI3 and PEI6 specimens. These high values result from more extra energy absorbed during the plastic deformation to initiate the crack, and the enhanced load transfer between epoxy rich area and adjacent fibre plies owing to the incorporation of CNCs. It is observed that the bridged fibres were deformed and eventually ruptured while necking was visible during the propagation of the delamination crack. Many vacant grooves and broken fibres are visible in PEI6 specimens (Fig. 7c,f). Nevertheless, rough surfaces with aggregates owing to the incorporation of a higher

CNCs content are observed, which could explain the presence of a decrease in load, thus the reduced $G_{IC,prop}$ value.

3.5.2. Mode II mechanisms

The fracture surfaces of PEI, PEI3, PEI6 tested specimens for Mode II as observed by SEM images are presented in Fig. 8. The formation of shear hackles at 45° relative to crack propagation plane is attributed to tensile microcracks in the epoxy matrix between adjacent carbon fibres [30]. Additionally, the rupture of carbon fibres has been observed for the PEI specimens during Mode II tests (see Fig. 8a,d; yellow and red arrows denote hackle and fibre ruptures, respectively). On the other hand, the shear hackles with a higher intensity present the larger effective surface area for PEI3 specimens, which absorb additional energy due to shear deformation during crack propagation (Fig. 8b,e). As the crack front interacts with the CNC aggregates that are regarded as "pins" (see dashed red oval in Fig. 8b,c), more extra energy is required to deform the aggregates [31]; thus contributing to the higher Mode II fracture energy for PEI3 and PEI6 specimens. Furthermore, matrix shear hackles with the highest intensity would also signify the largest fracture surface area among that of three types of specimens for PEI6 specimens (Fig. 8c,f). CNC aggregates and ruptured fibres also contribute to the highest G_{IIC} for 6 wt.% CNC-PEI nanofibrillar mat interleaved composites laminates.

4. Conclusions

In summary, this work reports an effective strategy for interlaminar toughening carbon fibre/epoxy composite laminates *via* the introduction of CNCs/PEI nanocomposites. Mode I and II interlaminar fracture energies of CNCs/PEI hybrid interleaved laminates can reach 310.0 ± 10.6 J/m^2 and 2.843 ± 0.111 kJ/m^2 respectively, showing 28% and 20% improvements over those of neat PEI specimens. In addition, the

tensile strength of CNCs-PEI hybrid nanofibrous mats increases up to 0.67 ± 0.13 MPa from 0.56 ± 0.09 MPa. Under Mode I loading, $G_{IC,ini}$ is enhanced on account of the synchronous mechanisms of larger effective fracture surface area and additional plastic strain by percolated networks of CNCs aggregates. In the case of Mode II loading, the cooperative toughening mechanism is a higher density of matrix shear hackles and pins by CNCs aggregates seen in CNCs-PEI hybrid interleaved composite laminates, thus providing the increased $G_{IIC,ini}$ values. The present work opens up a novel and promising area towards the development of cellulose nanocrystals-reinforced nanocomposites interleaved composite laminates with relatively high strength and fracture toughness for the inhibition of delamination cracks under Mode I and II loading, with additional merits of the sustainability of the precursor, large-scale availability at comparatively low cost in one-step fabrication process.

5. Acknowledgements

The authors would like to thank Prof. Ian Hamerton with the supply of commercial polyetherimide, Jean-Charles Eloi for assistance with the SEM images. Technical support from Advanced Composites Collaboration for Innovation and Science is much appreciated.

6. References

[1] S. Cauchi Savona, P.J. Hogg, Effect of fracture toughness properties on the crushing of flat composite plates, Compos. Sci. Technol. 66 (2006) 2317-2328.

[2] H. Zhang, A. Bharti, Z. Li, S. Du, E. Bilotti, T. Peijs, Localized toughening of carbon/epoxy laminates using dissolvable thermoplastic interleaves and electrospun fibres, Compos Part A Appl. Sci. Manuf. 79 (2015) 116-126.

[3] L. Li, C. Ortiz, A natural 3D interconnected laminated composite with enhanced

damage resistance, Adv. Funct. Mater. 25 (2015) 3463-3471.

[4] G.W. Beckermann, K.L. Pickering, Mode I and Mode II interlaminar fracture toughness of composite laminates interleaved with electrospun nanofibre mats, Compos Part A Appl. Sci. Manuf. 72 (2015) 11-21.

[5] M. Kuwata, P.J. Hogg, Interlaminar toughness of interleaved CFRP using non-woven mats: Part 1. Mode-I testing, Compos Part A Appl. Sci. Manuf. 42 (2011) 1551-1559.

[6] R.W. Hillermeier, J.C. Seferis, Interlayer toughening of resin transfer molding composites, Compos Part A Appl. Sci. Manuf. 32 (2001) 721-729.

[7] T.K. Tsotsis, Interlayer toughening of composite materials, Polym. Compos. 30 (2009) 70-86.

[8] N. Radacsi, F.D. Campos, C.R.I. Chisholm, K.P. Giapis, Spontaneous formation of nanoparticles on electrospun nanofibres, Nat. Commun. 9 (2018) 4740.

[9] Y. Dzenis, Structural nanocomposites, Science 319 (2008) 419.

[10] S. Hamer, H. Leibovich, A. Green, R. Avrahami, E. Zussman, A. Siegmann, D. Sherman, Mode I and Mode II fracture energy of MWCNT reinforced nanofibrillar mats interleaved carbon/epoxy laminates, Compos. Sci. Technol. 90 (2014) 48-56.

[11] V. Eskizeybek, A. Yar, A. Avcı, CNT-PAN hybrid nanofibrous mat interleaved carbon/epoxy laminates with improved Mode I interlaminar fracture toughness, Compos. Sci. Technol. 157 (2018) 30-39.

[12] P. Li, D. Liu, B. Zhu, B. Li, X. Jia, L. Wang, G. Li, X. Yang, Synchronous effects of multiscale reinforced and toughened CFRP composites by MWNTs-EP/PSF hybrid nanofibres with preferred orientation, Compos Part A Appl. Sci. Manuf. 68 (2015) 72-80.

[13] L. Chen, Q. Wang, K. Hirth, C. Baez, U.P. Agarwal, J.Y. Zhu, Tailoring the yield and characteristics of wood cellulose nanocrystals (CNC) using concentrated acid

hydrolysis, Cellulose 22 (2015) 1753-1762.

[14] R.J. Moon, A. Martini, J. Nairn, J. Simonsen, J. Youngblood, Cellulose nanomaterials review: structure, properties and nanocomposites, Chem. Soc. Rev. 40 (2011) 3941-94.

[15] A.K. Mohanty, S. Vivekanandhan, J.-M. Pin, M. Misra, Composites from renewable and sustainable resources: challenges and innovations, Science 362 (2018) 536.

[16] G. Gong, A.P. Mathew, K. Oksman, Toughening effect of cellulose nanowhiskers on polyvinyl acetate: Fracture toughness and viscoelastic analysis, Polym. Compos. 32 (2011) 1492-1498.

[17] Y. Zhai, K. Xiao, J. Yu, B. Ding, Closely packed x-poly(ethylene glycol diacrylate) coated polyetherimide/poly(vinylidene fluoride) fiber separators for lithium ion batteries with enhanced thermostability and improved electrolyte wettability, J. Power Sources 325 (2016) 292-300.

[18] J.J. Ge, D. Zhang, Q. Li, H. Hou, M.J. Graham, L. Dai, F.W. Harris, S.Z.D. Cheng, Multiwalled carbon nanotubes with chemically grafted polyetherimides, J. Am. Chem. Soc. 127 (2005) 9984-9985.

[19] S.J. Eichhorn, R.J. Young, The Young's modulus of a microcrystalline cellulose, Cellulose 8 (2001) 197-207.

[20] A. Tugrul Seyhan, M. Tanoglu, K. Schulte, Mode I and mode II fracture toughness of E-glass non-crimp fabric/carbon nanotube (CNT) modified polymer based composites, Eng. Fract. Mech. 75 (2008) 5151-5162.

[21] V. Kostopoulos, A. Kotrotsos, A. Baltopoulos, S. Tsantzalis, P. Tsokanas, T. Loutas, A.W. Bosman, Mode II fracture toughening and healing of composites using supramolecular polymer interlayers, Express Polym. Lett. 10 (2016) 914-926.

[22] C. Zhou, R. Chu, R. Wu, Q. Wu, Electrospun polyethylene oxide/cellulose nanocrystal composite nanofibrous mats with homogeneous and heterogeneous microstructures, Biomacromolecules 12 (2011) 2617-25.

[23] G. C. Nayak, R. Rajasekar, and C. K. Das, Effect of SiC coated MWCNTs on the thermal and mechanical properties of PEI/LCP blend, Compos Part A Appl. Sci. Manuf. 41 (2010) 1662-1667.

[24] T. Brugo and R. Palazzetti, The effect of thickness of Nylon 6,6 nanofibrous mat on Modes I–II fracture mechanics of UD and woven composite laminates, Compos. Struct. 154 (2016) 172-178.

[25] V. Kostopoulos, P. Karapappas, T. Loutas, A. Vavouliotis, A. Paipetis, P. Tsotra, Interlaminar fracture toughness of carbon fibre-reinforced polymer laminates with nano and micro-Fillers, Strain 47 (2011) 269-282.

[26] L. Daelemans, S. van der Heijden, I. De Baere, H. Rahier, W. Van Paepegem, K. De Clerck, Nanofibre bridging as a toughening mechanism in carbon/epoxy composite laminates interleaved with electrospun polyamide nanofibrous mats, Compos. Sci. Technol. 117 (2015) 244-256.

[27] F. Sacchetti, W.J.B. Grouve, L.L. Warnet, I.F. Villegas, Effect of resin-rich bond line thickness and fibre migration on the toughness of unidirectional carbon/PEEK joints, Compos Part A Appl. Sci. Manuf. 109 (2018) 197-206.

[28] J. George et al., Hybrid HPMC nanocomposites containing bacterial cellulose nanocrystals and silver nanoparticles, Carbohydr. Polym. 105 (2014) 285-292.

[29] Y. Habibi, L. A. Lucia, and O. J. Rojas, Cellulose nanocrystals: chemistry, self-assembly, and applications, Chem. Rev. 110 (2010) 3479-3500.

[30] L. Daelemans, S. van der Heijden, I. De Baere, H. Rahier, W. Van Paepegem, and

K. De Clerck, Using aligned nanofibres for identifying the toughening micromechanisms in nanofibre interleaved laminates, Compos. Sci. Technol. 124 (2016) 17-26.

[31] N. Zheng, Y. Huang, H.-Y. Liu, J. Gao, and Y.-W. Mai, Improvement of interlaminar fracture toughness in carbon fiber/epoxy composites with carbon nanotubes/polysulfone interleaves, Compos. Sci. Technol. 140 (2017) 8-15.

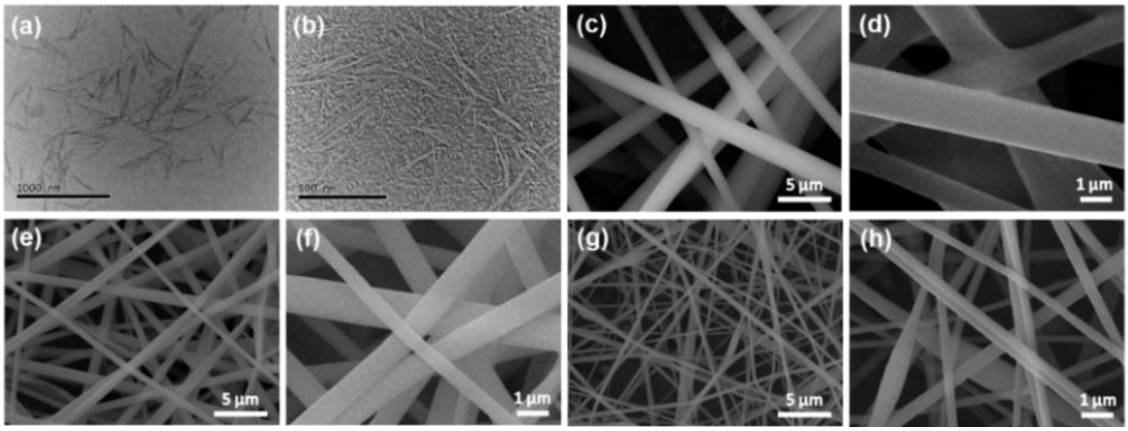

Fig. 1. Typical TEM images of CNCs at (a) high, (b) and low magnification, SEM images at two different levels of magnification of electrospun nanofibres: (c,d) PEI, (e,f) 3 wt.% CNC-PEI and, (g,h) 6 wt.% CNC-PEI.

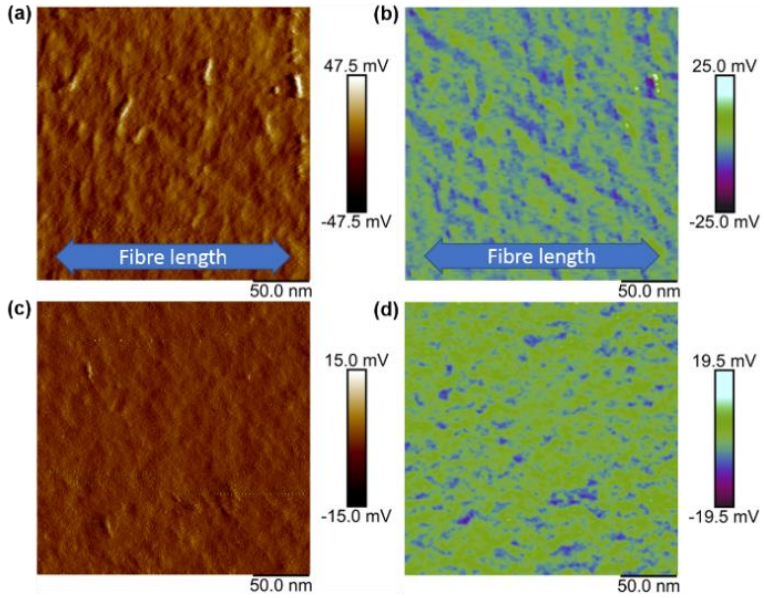

Fig. 2. High resolution AFM "error" and phase imaging of (a, b) longitudinal, and (c, d) transverse sections of electrospun 6 wt.% CNC-PEI nanofibres.

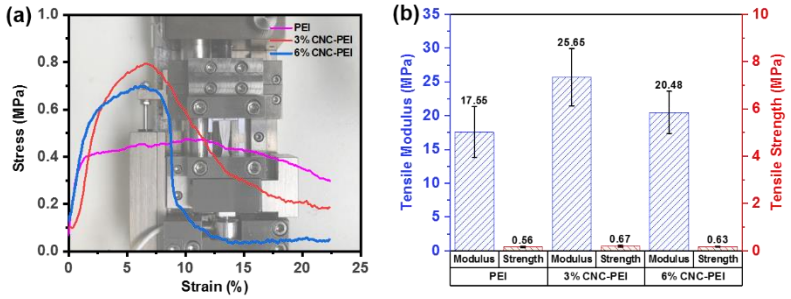

Fig. 3. (a) Tensile behaviour of nanofibrous mats, (b) tensile modulus and strength.

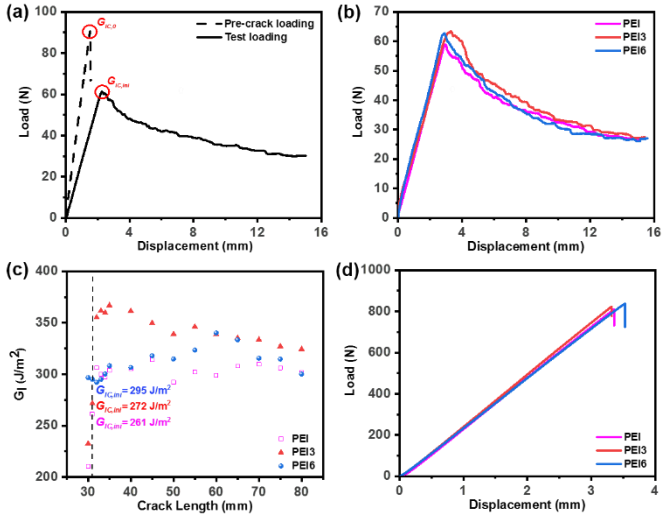

Fig. 4. (a) Representative load-displacement curves for PEI specimen with Mode I pre-crack loading and test loading, (b) typical load-displacement curves under test loading, (c) typical R-curves under Mode I test loading. The initiation fracture toughness value for each type of specimen has been labelled, (d) load-displacement curves for Mode II test.

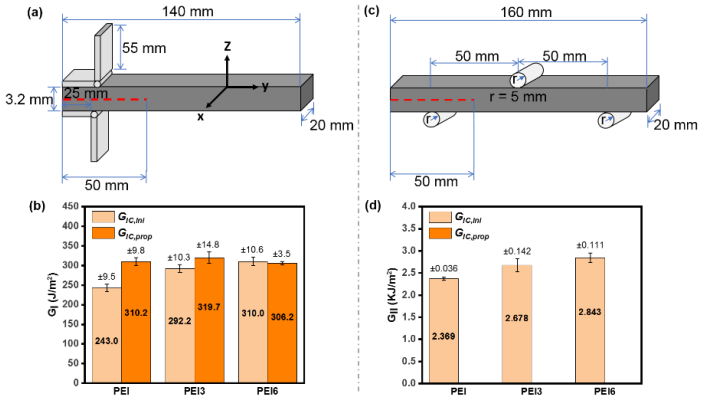

Fig. 5. Configuration and comparison of initiation and propagation energy release rate of PEI, PEI3, PEI6 specimens for (a,b) Mode I, (c,d) Mode II test.

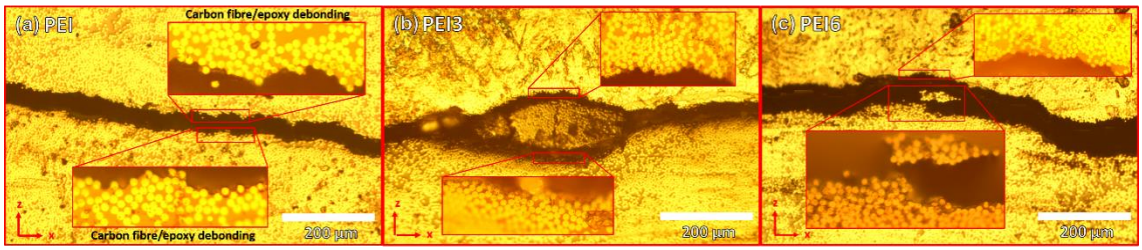

Fig 6. Cross-sectional images of DCB specimens (a) PEI, (b) PEI3, (c) PEI6.

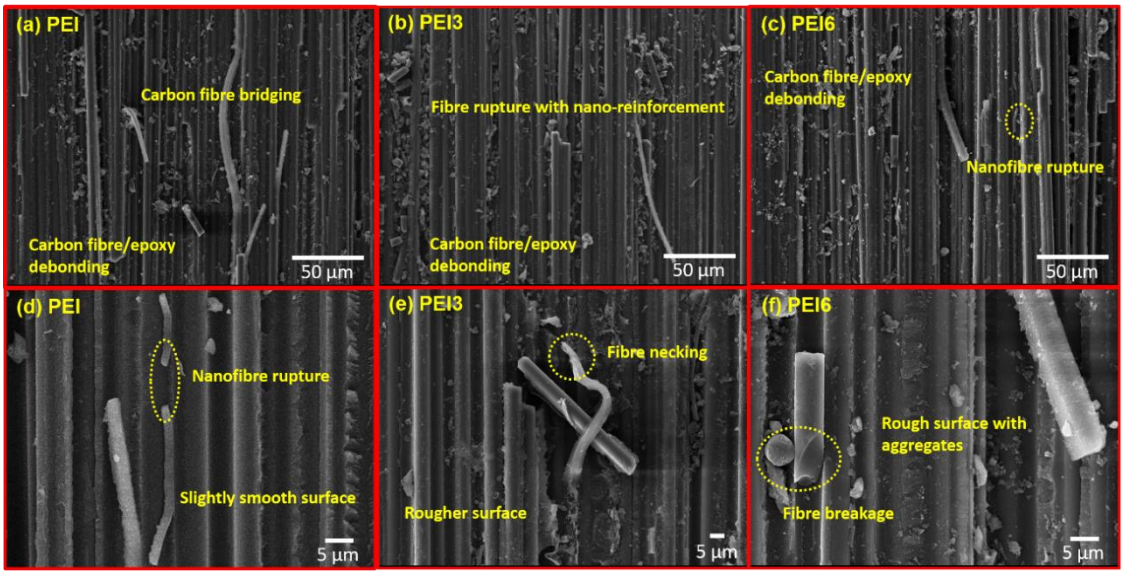

Fig. 7. SEM images of the Mode I fracture surfaces for (a,d) PEI, (b,e) PEI3, (c,f) PEI6 specimens at low and high magnification.

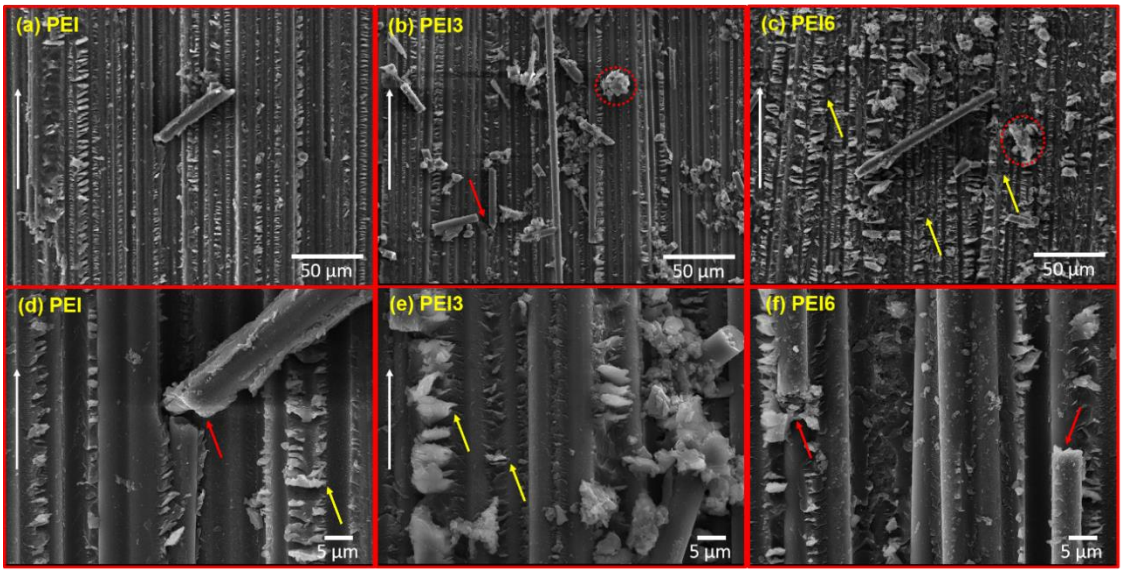

Fig. 8. SEM images of the Mode II fracture surfaces for (a,d) PEI, (b,e) PEI3, (c,f) PEI6 specimens. Delamination crack growth direction is indicated by white arrows.